Eu^{3+}@Organo-Si(HIPE) Macro-Mesocellular Hybrid Foams Generation: Syntheses, Characterizations, and Photonic Properties

Nicolas Brun,[†,‡] Beatriz Julián-López,*[,§] Peter Hesemann,[||] Guillaume Laurent,[⊥] Hervé Deleuze,[‡] Clément Sanchez,[†,⊥] Marie-France Achard,[†] and Rénal Backov*[,†]

Centre de Recherche Paul Pascal, UPR 8641-CNRS, 115 Avenue Albert Schweitzer, 33600 Pessac, France, Departamento de Química Inorgánica y Orgánica ESTCE, Universitat Jaume IAvda., Sos Baynat s/n12071 Castellón, Spain, UMR 5253, Institut Charles Gerhardt, Equipe AM2N, Ecole Nationale Supérieure de Chimie, 8 rue de l'Ecole Normale, 34296 Montpellier Cedex 05, France, Laboratoire de Chimie de la Matière Condensée de Paris, UMR-7574 CNRS, UPMC Université Paris 06, 4 Place Jussieu, France, and Institut des Sciences Moléculaires, UMR 5255-CNRS, Université Bordeaux 1, 351 Cours de la Libération, 33045 Talence Cedex, France

Received July 2, 2008. Revised Manuscript Received September 16, 2008

The elaboration of organosilica-based hybrid monoliths exhibiting a hierarchically structured bimodal porous structure with chelating functionality have been synthesized under interplay between high internal phase emulsion (HIPE) and lyotropic mesophases. For the first time grafted Eu^{3+}@*g*β-diketone-Si(HIPE) and Eu^{3+}@*g*malonamide-Si(HIPE) hybrid foams have been synthesized while a related Eu^{3+}@β-diketone-Si(HIPE) material has been obtained under a one-step co-condensation process. The loading of monoliths with lanthanides was performed by impregnation of an europium(III) salt in solution. The resulting materials have been thoroughly characterized via a large set of techniques including scanning electron microscopy (SEM), transmission electron microscopy (TEM), small angle X-ray scattering (SAXS), mercury porosimetry, nitrogen sorption isotherms, Fourier transform infrared (FTIR) spectroscopy, and ^{29}Si and ^{13}C magic angle spinning nuclear magnetic resonance (MAS NMR). This new series of luminescent Eu^{3+} containing Organo-Si(HIPE) materials has a large potential of promising applications in catalysis, optics, sensors, chromatographic supports, and so forth. For the first time, optical properties of these versatile materials with macro- and microporosity have been addressed thorough their absorption and emission spectra along with their relaxation luminescence properties.

Introduction

Recently, from the interface between bioinspired approaches,[1] hybrid organic−inorganic chemistry when extended to both soft chemistry in general (including organic polymer and supra-molecular chemistry) and complex fluids, has emerged the concept of "Integrative Chemistry"[2] where chemistry and process engineering are strongly coupled. Through the integrative chemistry synthetic pathways, the assembling of a large variety of molecular precursors or nanobuilding blocks into engineered hierarchical structures (bioinspired or not) should be strongly predictated in view of final function or polyfunctionalities to be reached. In this general context, current approaches to organize matter through a rational design are making the use of hierarchically organized reactors acting either in partitive or cooperative action modes.[2] These synthetic pathways include for instance the coupling of multiscale templating, self-assembled surfactant with larger templates as emulsion droplets,[3] foams,[4] latex beads,[5] bacterial threads,[6] organogelators,[7] controlled phase segregation,[8] nano- and macromolding,[9] and more

* Corresponding authors. E-mail: backov@crpp-bordeaux.cnrs.fr (R.B.); julian@qio.uji.es (B.J.-L.).
† UPR 8641-CNRS.
‡ Université Bordeaux 1.
§ Universitat Jaume IAvda.
|| Ecole Nationale Supérieure de Chimie.
⊥ UPMC Université Paris 06.

(1) (a) Mann, S.; Burkett, S. L.; Davis, S. A.; Fowler, C. E.; Mendelson, N. H.; Sims, S. D.; Walsh, D.; Whilton, N. T. *Chem. Mater.* **1997**, *9*, 2300. (b) Ozin, G. A *Chem. Commun.* **2000**, *6*, 419. (c) Soler-Illia, G. J. A. A.; Sanchez, C.; Lebeau, B.; Patarin, J. *Chem. Rev.* **2002**, *102*, 4093. (d) Sanchez, C.; Arribart, H.; Giraud-Guille, M. M. *Nat. Mater.* **2005**, *4*, 277. (e) Xu, A.-W.; Ma, Y.; Cölfen, H. *J. Mater. Chem.* **2007**, *17*, 415.
(2) (a) Backov, R *Soft Matter* **2006**, *2*, 452. (b) Prouzet, E.; Khani, Z.; Bertrand, M.; Tokumoto, M.; Guyot-Ferreol, V.; Tranchant, J.-F. *Microporous Mesoporous Mater.* **2006**, *1−3*, 369. (c) Sanchez, C.; Boissière, C.; Grosso, D.; Laberty, C.; Nicole, L *Chem. Mater.* **2008**, *3*, 682. (d) Prouzet, E.; Ravaine, S.; Sanchez, C.; Backov, R. *New J. Chem.* **2008**, *32*, 1284.
(3) Imhof, A.; Pine, D. J. *Adv. Mater.* **1998**, *10*, 697.
(4) (a) Chandrappa, G. T.; Steunou, N.; Livage, J. *Nature* **2002**, *416*, 702. (b) Maekawa, H.; Esquena, J.; Bishop, S.; Solans, C.; Chmelka, B. F. *Adv. Mater.* **2003**, *15*, 591. (c) Huerta, L.; Guillem, C.; Latorre, J.; Beltran, A.; Beltran, D.; Amoros, P. *Chem. Commun.* **2003**, 1448. (d) Carn, F.; Colin, A.; Achard, M.-F.; Deleuze, H.; Saadi, Z.; Backov, R. *Adv. Mater.* **2004**, *16*, 140. (e) Walsh, D.; Kulak, A.; Aoki, K.; Ikoma, T.; Tanaka, J.; Mann, S. *Angew. Chem., Int. Ed.* **2004**, *43*, 6691. (f) Carn, F.; Masse, P.; Saadaoui, H.; Julian, B.; Deleuze, H.; Ravaine, S.; Sanchez, C.; Talham, D. R.; Backov, R. *Langmuir* **2006**, *22*, 5469. (g) Carn, F.; Achard, M.-F.; Babot, O.; Deleuze, H.; Reculusa, S.; Backov, R. *J. Mater. Chem.* **2005**, *15*, 3887.
(5) (a) Holland, B. T.; Blanford, C. F.; Stein, A. *Science* **1998**, *281*, 538. (b) Antonietti, M.; Berton, B.; Göltner, C.; Hentzer, H.-P. *Adv. Mater.* **1998**, *10*, 154.
(6) Davis, S. A.; Burkett, S. L.; Mendelson, N. H.; Mann, S. *Nature* **1997**, *385*, 420.
(7) Llusar, M.; Roux, C.; Pozzo, J.-L.; Sanchez, C. *J. Mater. Chem.* **2003**, *3*, 442.
(8) Nakanishi, N. *J. Porous Mater.* **1997**, *4*, 67.
(9) (a) Yang, P.; Deng, T.; Zhao, D.; Feng, P.; Pine, D.; Scmelka, B. F.; Whitesides, G. M.; Stucky, G. D. *Science* **1998**, *282*, 2244. (b) Wang, D.; Caruso, R. A.; Caruso, F. *Chem. Mater.* **2001**, *13*, 364.

10.1021/cm8018023 CCC: $40.75
Published on Web 10/28/2008

recently breath figures.[10] Moreover, all previously mentioned morphosyntheses can be reached while employing external stimuli such as for instance electric or magnetic fields,[11] fluxes,[12] mechanical constraints,[13] imprinting,[14,1c]and so forth. During the last 10 years and beyond exclusive morphogenesis approaches, the synthesis of networks based on amorphous silica, eventually functionalized by organic groups, has particularly been studied. The resulting hybrid materials have opened an immense area in materials science that promotes extraordinary implications in the development of multifunctional materials.[15,16] Particularly, ordered macro-mesoporous materials are of interest for multiple applications in heterogeneous catalysis, separation techniques, absorbers, sensors, optics, and so forth. One way to generate defined architectures is to use either direct concentrated nonaqueous[17] or aqueous emulsions.[18] More recently, porous silica has been prepared through water/oil emulsions stabilized by silica nanoparticles in the absence of surfactants.[19] Indeed, different silica beds have been obtained by using emulsion−polymer double templates,[20] and their interest is specially related to their high internal surface. With this aim, our research group has developed a new process to obtain macrocellular silica monoliths with a high control on the final macroscopic cells (size and morphology) by varying the oil volume fraction of concentrated direct emulsions. This new series of silica porous networks was labeled SiHIPE[21] in regard to the first generation of porous organic polymer obtained through the use of concentrated reverse emulsions, porous polymers named Poly-HIPE, "high internal polymeric emulsion" phases[22a−d] later on extrapolated to hybrid interconnected polysilane/polystyrene foams.[22e,f] More recently we design the first generation of hybrid Si(HIPE) materials bearing molecular information.[23] This series of multiscale porous hybrid materials that we labeled Organo-Si(HIPE)[23] is able for instance to anchor and stabilize palladium nanoparticles depending on the organically derived silane precursor used in the syntheses yielding interesting cycling catalyts.[24]

Herein, we intend to take benefit of β-diketone and malolamide organosilane derivatives to complex lanthanide ions within new Organo-Si(HIPE) matrices. This ability allows these nondoped porous organo-Si(HIPE) materials to be suitable candidates for lanthanide and/or actinide extraction in the nuclear fuel cycle.[25] However, the direct and main application found for these organically modified silicates (ORMOSILs) is focused in photonics. As a result of their photophysical properties, the design of efficient lanthanide complexes as molecular devices became an important issue in the 1990s as their photophysical properties have grown considerably since Lehn[26] proposed the chelation of lanthanide ions with different ligand families. The lanthanide doped hybrid represents an important class of compounds in the development of advanced luminescent materials for nanophotonic and nanobiophotonic applications[27] such as laser materials[28] and luminescence labels,[29] efficient light-conversion molecular devices (LCMDs),[30] organic light-emitting devices (OLEDs),[31] and so forth. These rare-earth complexes give rise to sharp and intense emission lines upon ultraviolet light irradiation due to the lanthanide-centered luminescence generated from the effective intramolecular energy transfer from the coordinated ligands to the central lanthanide ion. This phenomenon is known as "antenna effect".[32] Luminescence properties of lanthanides organic

(10) Sakatani, Y.; Boissiere, C.; Grosso, D.; Nicole, L.; Soler-Illia, G.; Sanchez, C. *Chem. Mater.* **2008**, *20*, 1049.

(11) (a) Busch, S.; Dolhaine, H.; DuChesne, A.; Heinz, S.; Hochrein, O.; Laeri, F.; Podebrad, O.; Vietze, U.; Weiland, T.; Kniep, R. *Eur. J. Inorg. Chem.* **1999**, *10*, 1643. (b) Kniep, R.; Busch, S. *Angew. Chem., Int. Ed. Engl.* **1996**, *35*, 2624. (c) Terao, T.; Nakayama, T. *Phys. Rev. E* **1999**, *60*, 7157. (d) Grzybowski, B. A.; Stone, H. A.; Whitesides, G. M. *Nature* **2000**, *405*, 1033. (e) Assi, F.; Jenks, R.; Yang, J.; Love, C.; Prentiss, M. *J. Appl. Phys.* **2002**, *92*, 5584. (f) Carn, F.; Colin, A.; Schmitt, V.; Calderon, F.-L.; Backov, R. *Colloids Surf., A* **2005**, *263*, 341.

(12) (a) Biette, L.; Carn, F.; Maugey, M.; Achard, M.-F.; Maquet, J.; Steunou, N.; Livage, J.; Serier, S.; Backov, R. *Adv. Mater.* **2005**, *17*, 2970. (b) Serier, H.; Achard, M.-F.; Steunou, N.; Maquet, J.; Livage, J.; Babot, O.; Backov, R. *Adv. Funct. Mater.* **2006**, *16*, 1745. (c) Leroy, C. M.; Achard, M.-F.; Babot, O.; Steunou, N.; Masse, P.; Livage, J.; Binet, L.; Brun, N.; Backov, R. *Chem. Mater.* **2007**, *19*, 3988. (d) Dexmer, J.; Leroy, C. M.; Binet, L.; Heresanu, V.; Launois, P.; Steunou, N.; Coulon, C.; Maquet, J.; Brun, N.; Livage, J.; Backov, R. *Chem. Mater.* **2008**, *20*, 5541.

(13) Chronakis, I. S. *J. Mater. Process. Technol.* **2005**, *167*, 283.

(14) Li, Z.; Jaroniec, M. *J. Phys. Chem. B* **2004**, *108*, 824.

(15) (a) Sanchez, C.; Julian, B.; Belleville, P.; Popall, M. *J. Mater. Chem* **2005**, *15*, 3559. (b) Sanchez, C.; Soler-Illia, G. J. A. A.; Ribot, F.; Grosso, D. *C. R. Acad. Sci. Chim.* **2003**, *8*, 109.

(16) Sanchez, C.; Soler-Illia, G. J. A. A.; Ribot, F.; Lalot, T.; Mayer, C. R.; Cabuil, V. *Chem. Mater.* **2001**, *13*, 3061.

(17) (a) Imhof, A.; Pine, D. J. *Nature* **1997**, *389*, 948.

(18) Yi, G.-R.; Yang, S. M. *Chem. Mater.* **1999**, *11*, 2322.

(19) Binks, B. P. *Adv. Mater.* **2002**, *14*, 1824.

(20) Zhang, H.; Hardy, G. C.; Rosseinsky, M. J.; Copper, A. I. *Adv. Mater.* **2003**, *15*, 78.

(21) Carn, F.; Colin, A.; Achard, M.-F.; Deleuze, H.; Birot, M.; Backov, R. *J. Mater. Chem.* **2004**, *14*, 1370.

(22) (a) Barby, D.; Haq, Z. European Patent 0060138, 1982. (b) Cameron, N. R.; Sherrington, D. C. *High internal phase emulsions (HIPEs) Structure, properties and use in polymer preparation*; Advances in Polymer Science; Springer: Berlin/Heidelberg, 1996; Vol. 126, p 163. (c) Cameron, N. *Polymer* **2005**, *46*, 1439. (d) Zhang, H.; Cooper, A. I. *Soft Matter* **2005**, *2*, 107. (e) Tai, H.; Sergienko, H. A.; Silverstein, M. S. *Polymer* **2001**, *42*, 4473. (f) Silverstein, M. S.; Tai, H.; Sergienko, A.; Lumelsky, Y.; Pavlovsky, S. *Polymer* **2005**, *46*, 6682.

(23) Ungureanu, S.; Birot, M.; Guillaumme, L.; Deleuze, H.; Babot, O.; Julian-Lopez, B.; Achard, M.-F.; Sanchez, C.; Backov, R. *Chem. Mater.* **2007**, *19*, 5786.

(24) Ungureanu, S.; Deleuze, H.; Popa, M. I.; Sanchez, C.; Backov, R. *Chem. Mater.* **2008**, *20*, 6494.

(25) (a) Chan, G. Y. S.; Drew, M. G. B.; Hudson, M. J.; Iveson, P. B.; Liljenzin, J.-O.; Skalberg, M.; Spjuth, L.; Madic, C. *J. Chem. Soc., Dalton Trans.* **1997**, 649. (b) Bourg, S.; Broudic, J.-C.; Conocar, O.; Moreau, J. J. E.; Meyer, D.; Wong Chi Man, M. *Chem. Mater.* **2001**, *13*, 491.

(26) Lehn, J. M. *Angew. Chem.* **1990**, *102*, 1347.

(27) (a) Meng, Q.; Boutinaud, P.; Zhang, H.; Mahiou, R. *J. Lumin.* **2007**, *124*, 15. (b) Li, H. R.; Lin, J.; Zhang, H. J.; Fu, L. S.; Meng, Q. G.; Wang, S. B. *Chem. Mater.* **2002**, *14*, 3651. (c) Escribano, P.; Julian-Lopez, B.; Planelles-Arago, J.; Cordoncillo, E.; Viana, B.; Sanchez, C. *J. Mater. Chem.* **2008**, *18*, 23.

(28) Yokoyama, H. *Science* **1992**, *256*, 66.

(29) (a) Richardson, F. S. *Chem. Rev.* **1982**, *82*, 541. (b) Buonocore, G. E.; Li, H.; Marciniak, B. *Coord. Chem. Rev.* **1990**, *99*, 55.

(30) (a) Li, S.; Song, H.; Li, W.; Ren, X.; Lu, S.; Pan, G.; Fan, L.; Yu, H.; Zhang, H.; Qin, R.; Dai, Q.; Wang, T. *J. Phys. Chem. B* **2006**, *110*, 23164. (b) Farias, R. F.; Alves, S., Jr.; Belian, M. F.; Sa, G. F. *J. Colloid Interface Sci.* **2001**, *243*, 523.

(31) Zheng, Y.; Fu, L.; Zhou, Y.; Yu, J.; Yu, Y.; Wang, S.; Zhang, H. *J. Mater. Chem.* **2002**, *12*, 919.

(32) (a) Klonkowski, A. M.; Lis, S.; Pietraszkiewicz, M.; Hnatejko, Z.; Czarnobaj, K.; Elbanowski, M. *Chem. Mater.* **2003**, *15*, 656. (b) Sabbatini, N.; Guardigli, M.; Manet, I.; Ungaro, R.; Casnati, A.; Ziessel, R.; Uldrich, G.; Asfari, Z.; Lehn, J. M. *Pure Appl. Chem.* **1995**, *67*, 135.

complexes anchored onto (or within porous) solid materials[33] as core−shell or nanostructures particles,[34] mesoporous solids,[35] have been drastically studied due to the quantum confinement effect of the photophysical properties that can be modified and tuned.[36] In this general context, we present herein for the first time lanthanide derivatives Eu^{3+}@Organo-Si(HIPE) macro-mesocellular foam syntheses and their characterization together with the determination of their luminescent properties. Two sets of materials were prepared. The first set was obtained from a two-step process in which β-diketone or malonamide organosilane derivates were grafted to a previously prepared macrocellular Si(HIPE). A third material was obtained via a one-pot co-condensation of the silica precursor (tetraethyl-orthosilane, TEOS) and a trialcoxysilylated β-diketone precursor. Luminescence studies of the Eu^{3+}-impregnated materials were carried out to get information about the lanthanide environment, the efficiency in the complexation depending on the synthetic strategy, and their suitability as luminescent material.

Experimental Section

Materials. Ethyl malonate monoamide, ethyl acetate, and triethoxyvinylsilane have been purchased from Fluka. (3-Aminopropyl)triethoxysilane and dibenzo-18-*crown*-6 (98%) have been purchased from Janssen Chimica. 4-Bromoacetophenone (98%), sodium hydride (57−63%) oil dispersion, palladium acetate, and tetradecyltrimethylammonium bromide (98%,TTAB) have been purchased from Alfa Aesar. Tetraethylorthosilane (98%, TEOS) and europium nitrate pentahydrate have been purchased from Aldrich. Dodecane (99%) was purchased from Rectapur. HCl (37%) was purchased from Analar Normapur. The reactants were used as received without further purification, except (3-aminopropyl)triethoxysilane and triethoxyvinylsilane, which were distilled before use.

Syntheses. *Triethoxysilylated Precursors Synthesis.* N1-(3-(triethoxysilyl)propyl)malonamide (**1**) was prepared by coupling of ethyl malonate monoamide with (3-aminopropyl)triethoxysilane as described in the literature.[37] 1-[4-(2-Triethoxysilyl-vinyl)-phenyl]-butane-1,3-dione (**2**) was synthesized in a two step sequence as already described for the synthesis of related 1-phenyl-3-[4-(2-triethoxysilyl-vinyl)-phenyl]-propane-1,3-dione.[38]

First, 1-[4-bromophenyl]-butane-1,3-dione was prepared by a Claisen condensation of ethyl acetate and 4-bromoacetophenone.[39] Silylation was then achieved by coupling of 1-[4-bromophenyl]-butane-1,3-dione with vinyl-triethoxysilane under Heck reaction conditions. 1-[4-(2-Triethoxysilyl-vinyl)-phenyl]-butane-1,3-dione (**2**), 1-[4-bromophenyl]-butane-1,3-dione (5.00 g/20.7 mmol), palladium acetate (22.4 mg/0.1 mmol), and P(o-$CH_3C_6H_4$)$_3$ (182 mg/0.6 mmol) were placed in a two necked flask under argon. Freshly distilled DMF (50 mL), triethylamine (8.8 mL/63 mmol), and triethoxyvinylsilane (4.80 g/25mmol) were added. The resulting homogeneous solution was heated to 100 °C. After 18 h at this temperature, the reaction mixture was allowed to cool to room temperature and filtered. The solvents were pumped off, and the resulting heterogeneous residue was dissolved in diethyl ether. Filtration and evaporation of the solvent gave the product as highly viscous orange oil. Yield: 6.84 g/19.5 mmol (93%).^{1}H NMR ($CDCl_3$): δ 1.25 (t, 9H, J = 7.0 Hz), 2.17 (s, 3H), 3.87 (q, 6H, J = 7.0 Hz), 6.15 (s, 1H), 6.27 (d, 1H, J = 19.3 Hz), 7.21 (d, 1H, 19.4 Hz), 7.48−7.53 (m, 2H), 7.81−7.86 (m, 2H), 11.69 (bs, 1H). ^{13}C NMR ($CDCl_3$): δ 18.2, 25.9, 58.7, 96.7, 121.0, 126.9, 127.3, 134.7, 141.2, 147.7, 182.3, 194.0. FT-IR (KBr) ν_{max}/cm^{-1} 2975, 2926, 2887, 1606, 1295, 1167, 1080, 962, 829, 783. HRMS [FAB] calcd for $C_{18}H_{27}O_5Si$ $(M + H)^+$, 351.1627; found, 351.1617.

Native-Si(HIPE) Synthesis. Typically, 5 g of TEOS is added to 16 g of a TTAB aqueous solution at 35 wt % previously acidified (7 g of HCl), and hydrolysis is allowed to take place until a monophasic hydrophilic medium is obtained. The oily phase constituted of 35 g of dodecane is then emulsified drop by drop into the hydrophilic continuous phase using a mortar. The emulsion is then allowed to condense for 1 week at room temperature. The as-synthesized monolith is washed three times with a tetrahydrofuran/acetone mixture (at 50 vol %) to extract the oily (dodecane) phase from the monolith. The drying of the material during a week at room temperature is followed by further thermal treatment at 650 °C for 6 h (heating rate of 2 °C/min), with a first plateau at 200 °C for 2 h, to both remove the mesoscale organic supramolecular-type templates and gently sinter the inorganic network.

g*Organo-Si(HIPE) Synthesis by Grafting Method.* A piece of native-Si(HIPE) (0.3 g) is added into a solution of N1-(3-(triethoxysilyl)propyl)malonamide (0.92 g, 0.003 mol) or 1-[4-(2-triethoxysilyl-vinyl)-phenyl]-butane-1,3-dione (1.05 g, 0.003 mol) in 100 mL of a toluene/chloroform mixture (at 70 vol %/30 vol %). For a good impregnation, the suspension is placed under vacuum, until the effervescence disappears. After 24 h aging at room temperature, the solution is filtrated. The monoliths are then washed three times with 100 mL of a toluene/chloroform mixture (at 70 vol %/30 vol %) and dried in air. Resulting monoliths are called gMalonamide-Si(HIPE) and $g\beta$-diketone-Si(HIPE).

Organo-Si(HIPE) Synthesis by Co-Condensation Reaction. In a typical synthesis, 4 g of TEOS and 1 g of 1-[4-(2-triethoxysilyl-vinyl)-phenyl]-butane-1,3-dione are introduced in 16 g of a TTAB aqueous solution at 35 wt % previously acidified (7 g of HCl), and hydrolysis is allowed to take place until a monophasic hydrophilic medium is obtained. The oily phase constituted of 35 g of dodecane is then emulsified drop by drop into the hydrophilic continuous phase using a mortar. The emulsion is then allowed to condense for 1 week at room temperature. The as-synthesized monolith is washed three times with a tetrahydrofuran/acetone mixture (at 50

(33) (a) Quach, A.; Escax, V.; Nicole, L.; Goldner, P.; Guillot-Noel, O.; Aschehoug, P.; Hesemann, P.; Moreau, J.; Gourier, D.; Sanchez, C. *J. Mater. Chem.* **2007**, *17*, 2552. (b) Crepaldi, E. L.; Soler-Illia, G.; Grosso, D.; Albouy, P. A.; Sanchez, C. *Chem. Commun.* **2001**, 1582.
(34) (a) Liu, G.; Hong, G.; Sun, D. *J. Colloid Interface Sci.* **2004**, *278*, 133. (b) Bazzi, R.; Flores, M. A.; Louis, C.; Lebbou, K.; Zhang, W.; Dujardin, C.; Roux, S.; Mercier, B.; Ledoux, G.; Bernstein, E.; Perriat, P.; Tillement, O. *J. Colloid Interface Sci.* **2004**, *273*, 191. (c) Meng, Q. G.; Boutinaud, P.; Franville, A. C.; Zhang, H. J.; Mahiou, R. *Microporous Mesoporous Mater.* **2003**, *65*, 127.
(35) (a) Castro, Y; Julian, B.; Boissiere, C.; Viana, B.; Amenitsch, H.; Grosso, D; Sanchez, C. *Nanotechnology* **2007**, 18. (b) Castro, Y.; Julian-Lopez, B.; Boissiere, C.; Viana, B.; Grosso, D.; Sanchez, C. *Microporous Mesoporous Mater.* **2007**, *103*, 273. (c) DeOliveira, E.; Neri, C. R.; Serra, O. A.; Prado, A. G. S *Chem. Mater.* **2007**, *19*, 5437.
(36) (a) Tan, M.; Ye, Z.; Wang, G.; Yuan, J. *Chem. Mater.* **2004**, *16*, 2494. (b) Nassar, E. J.; Neri, C. R.; Calefi, P. S.; Serra, O. A. *J. Non-Cryst. Solids* **1999**, *247*, 124. (c) Gomes, J.; Pires, A. M.; Serra, O. A. *J. Fluoresc.* **2006**, *16*, 411. (d) Sun, S.; Murray, C. B. *J. Appl. Phys.* **1999**, *85*, 4325. (e) Wang, W.; Widiyastuti, W.; Ogi, T.; Lenggoro, I. W.; Okuyama, K. *Chem. Mater.* **2007**, *19*, 1723.
(37) Broudic, J.-C.; Conocar, O.; Moreau, J. J. E.; Meyer, D.; Wong Chi Man, M. *J. Mater. Chem.* **1999**, *9*, 2283.
(38) Banet, P.; Legagneux, L.; Hesemann, P.; Moreau, J. J. E.; Nicole, L.; Quach, A.; Sanchez, C.; Tran-Thi, T.-H. *Sens. Actuators B* **2008**, *130*, 1.
(39) Popic, V. V.; Korneev, S. M.; Nikolaev, V. A.; Korobitsyna, I. K. *Synthesis* **1991**, 195.

vol %) to extract the oily (dodecane) phase from the monolith. The drying of the material during a week at room temperature is followed by further thermal treatment at 180 °C for 6 h (heating rate of 2 °C/min) to favor solvent evaporation and the consolidation of the networks. The as-synthesized monolith is called β-diketone-Si(HIPE). In the same way we have tried to synthesize through a one-pot co-condensation route the material "Malonamide-Si(HIPE)", this without any success either varying the pH (basic condition and not acidic), NaF salt effect to tune the condensation process, or lyophilization to dry the compound while avoiding structural collapse (sublimation of ice). Despite all our attempts we never obtained a self-standing porous monolith-type material.

$Eu(NO_3)_3 \cdot 5H_2O$ Impregnation. A piece of functionalized-Si-(HIPE) support (0.15 g), is placed in a solution of $Eu(NO_3)_3 \cdot 5H_2O$ (2.14 g, 0.005 mol) in 100 mL of a isopropanol/ethanol mixture (at 50 vol %). To help fill up the porous matrices, a vacuum is applied until the disappearing of the effervescence. Then, the imbibed monoliths are left for 1 week at room temperature under static vacuum. After Eu^{3+} impregnation the hybrid materials were washed three times with an isopropanol/ethanol mixture (at 50 vol %) and dried in air. Resulting monoliths are called either Eu@Organo-Si(HIPE) when the organic functionalization was provided through a one step co-condensation process or Eu@*g*Organo-Si(HIPE) when the organic counterpart is generated through a grafting process, the "*g*" leading for "grafted".

Characterizations. Transmission electron microscopy (TEM) experiments were performed with a Jeol 2000 FX microscope (accelerating voltage of 200 kV). The samples were prepared as follows: silica scaffolds in a powder state were deposited on a copper grid coated with a Formvar/carbon membrane. Scanning electron microscopy (SEM) observations were performed with a Jeol JSM-840A scanning electron microscope operating at 10 kV. The specimens were gold-coated or carbon-coated prior to examination. Surface areas and pore characteristics at the mesoscale were obtained with a Micromeritics ASAP 2010. Intrusion/extrusion mercury measurements were performed using a Micromeritics Autopore IV apparatus to reach the scaffold macrocellular cell characteristics. X-ray diffraction experiments were carried on a 18 kW rotating anode X-ray source (Rigaku-200) with use of Ge(111) crystal as monochromator. The scattered radiation, to obtain the small angle X-ray Scattering (SAXS) information, was collected on a two-dimensional detector (Imaging Plate system from Mar Research, Hamburg). The sample−detector distance was 500 mm. Thermogravimetric analyses (TGA) were carried out under an oxygen flux (5 $cm^3 \cdot min^{-1}$) using a heating rate of 5 $°C \cdot min^{-1}$. The apparatus is a Stearam TAG-1750 thermogravimetric analyzer. The Fourier transform infrared (FTIR) spectra have been obtained with a Nicolet 750 FTIR spectrometer. Nuclear magnetic resonance (MRN) spectra were recorded on a Bruker Avance 300 spectrometer (7 T) operating at 75.5 MHz for ^{13}C and 59.6 MHz for ^{29}Si. The ^{13}C cross-polarization magic angle spinning nuclear magnetic resonance (CP MAS NMR) spectrum was performed with $\omega_{1I}/2\pi$ and $\omega_{1S}/2\pi$ equal to 50 kHz, a recycling delay of 1 s, a contact time of 1 ms, in a rotor of 4 mm spinning at 14 kHz. ^{29}Si CP MAS NMR spectra were performed with $\omega_{1I}/2\pi$ and $\omega_{1S}/2\pi$ equal to 50 kHz, a recycling delay of 1 s, and a contact time of 3 ms, in a rotor of 4 mm spinning at 5 kHz. ^{1}H TPPM15 decoupling (two pulse phase modulation)[40] at $\omega_{1I}/2\pi$ equal to 50 kHz was applied in both cases during acquisition but not during recycling. ^{29}Si sites are labeled with the conventional T_n and Q_n notation. T refers to functional $(R)SiO_3$- units and Q to SiO_4- units, and *n* is the number of bridging oxygen atoms surrounding the silicon. Chemical shifts were determined relative to TMS (tetramethylsilane). The spectra were deconvoluted with the DMFIT program.[41]

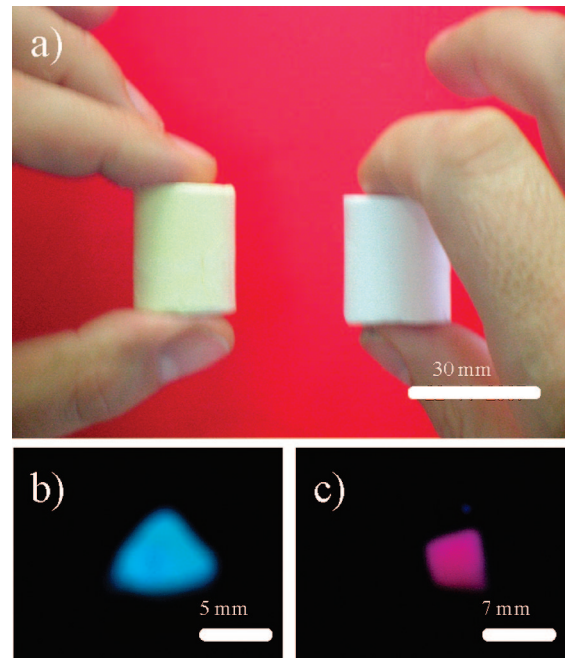

Figure 1. As-synthesized Organo-Si(HIPE) monoliths. (a) Eu^{3+}@$g\beta$-diketone-Si(HIPE) (bearing the yellow color of the β-diketone silane derivative) and Eu^{3+}@*g*malonamide-Si(HIPE) (white as malonamide silane derivative is colorless), (b) Eu^{3+}@*g*malonamide-Si(HIPE) when irradiated under UV light (350 nm), and (c) Eu^{3+}@$g\beta$-diketone-Si(HIPE) when irradiated under UV light (350 nm).

The UV−vis absorption measurements of the samples were performed at room temperature on a Varian Cary 5 spectrophotometer, in the 200−900 nm range. Excitation and emission spectra were obtained with a Cary Eclipse model (Varian) spectrofluorimeter. The excitation spectra were recorded from 200 to 600 nm for an emission wavelength of 615 nm, corresponding to the $^5D_0 \rightarrow {}^7F_2$ Eu^{3+} transition. The emission spectra were registered from 410 to 750 nm upon excitation at 396 nm ($^5D_0 \rightarrow {}^5L_6$ Eu^{3+} transition). In the excitation/emission profiles, a normalization process was performed for a better comparison of the relative intensities of the bands. This process consists of the selection of one band as a reference and the multiplication or division of all the spectra by a numerical value to get the same intensity for this band in all the curves. Lifetime values were extracted by fitting the decay curves.

Results and Discussion

Herein we make use of both a co-condensation ("one-pot") process where the silylated precursors $(R\text{-}Si(OEt)_3)$ are incorporated into the reaction medium and participates in the whole synthesis and a two step grafting process where the precursor is covalently grafted onto the preformed native inorganic Si(HIPE) (see Experimental Section for synthetic details). From each synthetic pathway we obtained self-standing monolith-type materials showing luminescent properties upon UV light exposure (Figure 1). The monolith macroporosity is obtained through the use of a concentrated direct emulsion, that is, dispersion of oil in water where the

(40) Bennett, A. E.; Rienstra, C. M.; Auger, M.; Lakshmi, K. V.; Griffin, R. G. *J. Chem. Phys.* **1995**, *103*, 6951.

(41) (a) Harris, R. K.; Robbins, M. L. *Polymer* **1978**, *19*, 1123. (b) Babonneau, F. *New J. Chem.* **1994**, *18*, 1065. (c) Chevalier, Y.; Grillet, A.-C.; Rahmi, M.-I.; Lière, C.; Masure, M.; Hémery, P.; Babonneau, F. *Mater. Sci. Eng. C* **2002**, *21*, 143.

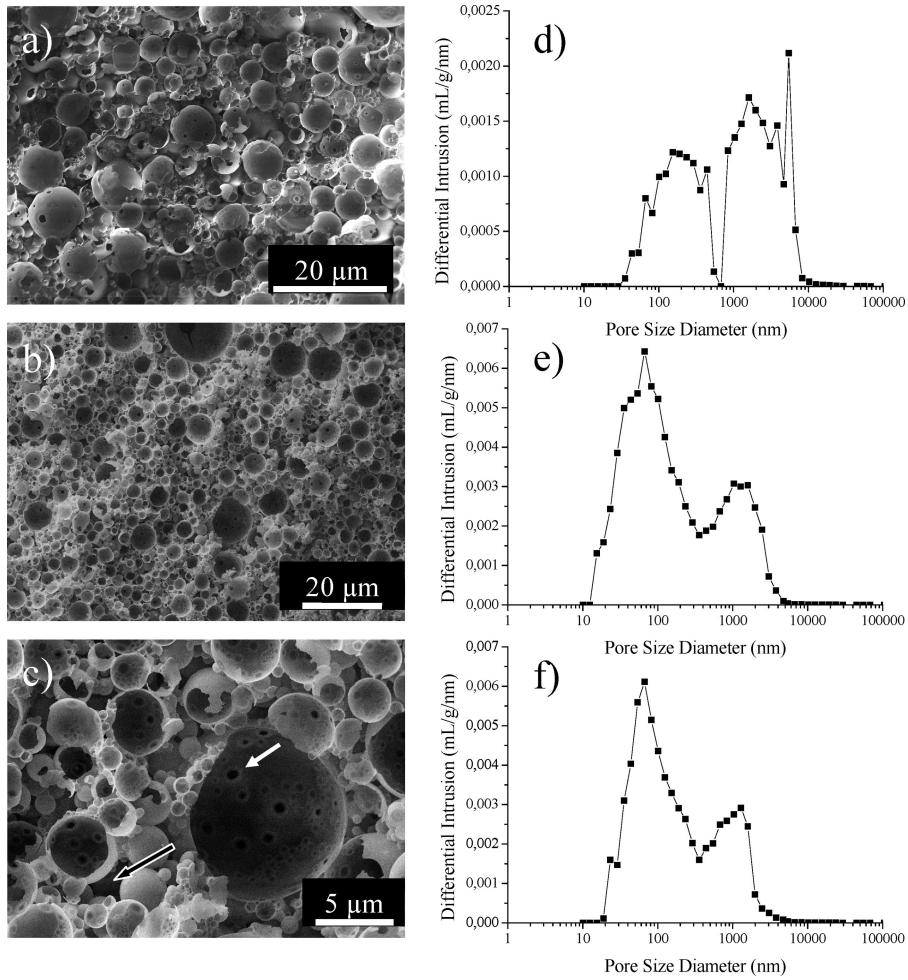

Figure 2. SEM micrographs: (a) $Eu^{3+}@\beta$-diketone-Si(HIPE), (b) $Eu^{3+}@g\beta$-diketone-Si(HIPE), and (c) $Eu^{3+}@g\beta$-diketone-Si(HIPE), magnification of b. Macroscopic pore size distribution obtained through mercury intrusion porosimetry: (d) $Eu^{3+}@\beta$-diketone-Si(HIPE), (e) $Eu^{3+}@g\beta$-diketone-Si(HIPE), and (f) $Eu^{3+}@g$malonamide-Si(HIPE). The white arrow indicates internal cell junction; the black arrow indicates external cell junction.

continuous phase will be the hydrophilic media containing the hydrolyzed precursors.

The first observation emerging from scanning electron microscopy (SEM) basic observations (Figure 2 a−c) is that the macroscopic void spaces are rather polydisperse in size, ranging from 1 μm up to 10 μm, and that there is no significant differences in materials morphology upon the synthetic pathways in use, one-pot co-condensation or two-step grafting procedures. The macroscopic textures of the monoliths resemble a "hollow spheres" aggregation.

As previously used to generate the inorganic Si-HIPE0.035,[21] the high acidic concentration (pH close to 0.035) yields the silica far from its isoelectric point and therefore the native object will depict a strong Euclidian character (basically, Euclidien character is dedicated to objects where the density is constant when increasing their size, contrary to the ones bearing a fractal character where the density is decreasing as the objects' size is increasing).[42] Also, as mentioned before,[21] it is obvious that mineralization starts at the oil/water interface and then extends to the aqueous hydrophilic phase, the interface acting as a defect where the nucleation enthalpy will be lowered. Beyond SEM observations it is important to provide more quantitative information related with the macroporosity, as for instance bulk and skeleton densities. With this purpose, we performed mercury porosimetry (Figure 2 d−f). The first information of importance for further applications is the fact that these as-synthesized materials possess mechanical strength high enough to support mercury impregnation. Also, it is worth mentioning that mercury porosimetry provides information only on the void spaces that support the most the mercury impregnation, that is, the windows that connect two adjacent macropores, rather than the macropore themselves. As previously observed for the inorganic Si-HIPE series,[21] we obtain two set of windows (Figure 2c). First we have the windows that intrinsically connect two adjacent macropores, that we have previously called "internal junctions".[21] Also, considering the aggregated "hollow spheres" textural aspect of the macropores, we have to consider windows emerging from aggregation between several hollow spheres previously called "external junctions".[21] At that point, it is expected to get two main contributions when considering the cell-junction diameter distribution data, and this effect is clearly seen in Figure 2 d−f. Specific morphological characteristics (percentage of porosity, bulk, and wall densities) of these hybrid compounds can be found in Table 1.

(42) Brinker, C. J.; Scherer G. W. *Sol-Gel Science: the Physics and Chemistry of Sol-Gel Processing*; Academic Press: San Diego, 1990.

Table 1. Mercury Intrusion Porosimetry Data

	material		
	Eu^{3+}@β-diketone-Si(HIPE)	Eu^{3+}@$g\beta$-diketone-Si (HIPE)	Eu^{3+}@ *g*malonamide-Si(HIPE)
intrusion volume ($cm^3 \cdot g^{-1}$)	11.2	9.2	6.6
porosity (%)	95.4	76.6	60.9
bulk density ($g \cdot cm^{-3}$)	0.08	0.08	0.09
wall density ($g \cdot cm^{-3}$)	1.84	0.35	0.24

Table 2. Hybrid Monoliths Surface Area Calculated from both the BET and BJH Methods[a]

	material		
	Eu^{3+}@β-diketone-Si(HIPE)	Eu^{3+}@$g\beta$-diketone-Si (HIPE)	Eu^{3+}@ *g*malonamide-Si(HIPE)
BET ($m^2 \cdot g^{-1}$)	275	360	150
BJH ($m^2 \cdot g^{-1}$)	95	87	22
total pore volume ($cm^3 \cdot g^{-1}$)	0.14	0.20	0.08

[a] The BJH method is applied only to pore sizes higher than 17 Å diameter and for the desorption curve.

We can notice from data gathered in Table 1 that these as-synthesized hybrid porous networks are bearing bulk densities around 0.08 $g \cdot cm^{-3}$ which are comparable with those of silica aerogel.[43] Differences of the plateau border densities are also observed between the grafted and the co-condensed materials. This feature is indeed in agreement with the hybrid compounds stoichiometry; as for the co-condensed materials, which are bearing the higher wall densities, we have introduced three times more organic functions when compared with the grafted compounds (see Table 3) and also two times more europium ions. Also, the plateau borders (the macroscopic walls) of all compounds are micro/mesoporous (see later in the text). This feature, together with the fact that the grafted compounds are bearing a low amount of organic moieties and europium species, is inducing the relatively low skeletal densities obtained for the grafted compounds (around 0.3 g cm^{-3}), below the silica density. Moreover, the macroscopic length scale porosity is also higher for the one-pot β-diketone material than the other two solids obtained by grafting techniques. This feature reflects that the one-pot co-condensation route is inducing a lower stability of the oil/water interfaces of the direct emulsions in use. The synergetic effect between the tetradecyl-trimethylamonium bromide (TTAB) lyotropic mesophase and the β-diketone precursors is thereby minimizing the oil/water interface stability (optimizing coalescence). In consequence both external and internal junctions are switched to the higher values for the higher for the one-pot β-diketone material (Figure 2d), when compared with the grafted compounds (Figure 2e,f). The use of surfactant, herein the TTAB, is indeed very important for two main reasons. First, the surfactant stabilizes the oil/water interface of the direct emulsion, that is, like all emulsions, direct or reverse and concentrated or not, a metastable thermodynamic system where Ostwald ripening and coalescence induced macroscopic phase separation. Second, the use of lyotropic mesophases will create, as it the case for mesoporous compounds,[44] supramolecular assembly that will promote ordered porosity at the mesoscopic length scales. Here again for the one pot co-condensation route, we cannot exclude a synergetic effect between the TTAB entities and the β-diketone precursors acting as a cosurfactant.[45] Considering the materials presented herein, the first experiment that is of help to reveal the periodically organized mesoporosity is the transmission electron microscopy (TEM), Figure 3. As observed in Figure 3a−c the macrocellular foam mesoporosity is hexagonally organized whatever the methodology of preparation in use, either by grafting or via a co-condensation route. Thereby, it is important to have a close look of the hexagonal unit cell extracted from the SAXS experiments (Figure 3e,f). Typically, a first peak is observed for 6.5 nm (0.095 $Å^{-1}$) associated with two other contributions at 3.9 nm (0.159 $Å^{-1}$) and 3.4 nm (0.185 $Å^{-1}$). The presence of these last two peaks suggests hexagonal organization of the channels, and it has been reported that SAXS spectrum of powdery hexagonal mesoporous materials exhibits a typical three peak pattern, associated with a first feature at low angle (100 reflection line) and two other peaks at higher angles (110 and 200 reflections lines).[46] These three reflection lines can be assigned to a hexagonal unit cell ($a_0 = 2d_{100}/3^{1/2}$) that corresponds to the sum of the pore diameter and the pore wall thickness. According to Bragg's law, the unit cell dimension (a_0) for these compounds is found to be the same and equals 7.6 nm, in good agreement with previous results concerning the first Organo-Si(HIPE) generation.[23]

To better describe the mesoscale void space organizations and quantify the specific surface areas, nitrogen adsorption−desorption measurements were performed at 77 K. All the nitrogen adsorption−desorption curves and the associated mesopore size distributions are presented in Figure 4. In a general manner, N_2 adsorption curves rise rapidly in the low relative pressure range (0 to 0.3) indicating microporosity. Above relative pressure of 0.3 and up to 1.0, a weak hysteresis loop can be observed between the adsorption and desorption curves that confirmed the presence of mesopore within the different samples.

Table 2 summarizes the specific surface areas of the different thermally treated hybrid monoliths when using both the BET and the BJH methods. We can consider that the hybrid compounds are essentially microporous (pores sizes below 17 Å) associated to some degree of mesoporosity (pore sizes higher than 17 Å). Also, pore size distributions have been expressed using the density functional theory (DFT) method (Figure 4d−f) and appear to be almost identical for the three materials and in good relation with what was observed and extracted from the nitrogen physisorption experiments. Indeed all the calculated pore size distributions

(43) Soleimani Dorcheh, A.; Abbasi, M. H. *J. Mater. Proc. Technol.* **2008**, *199*, 10 (and references within).

(44) (a) Kresge, C. T.; Leonowicz, M. E.; Roth, W. J.; Vartuli, J. C.; Beck, J. S. *Nature* **1992**, *359*, 710. (b) Beck, J. S.; Vartuli, J. C.; Roth, W. J.; Leonowicz, M. E.; Kresge, C. T.; Schmitt, K. D.; Chu, C. T.-W.; Olson, D. H.; Sheppard, E. W.; McCullen, S. B.; Higgins, J. B.; Schlenker, J. L. *J. Am. Chem. Soc.* **1992**, *114*, 10834.

(45) Nicole, L.; Boissière, C.; Grosso, D.; Heseman, P.; Moreau, J.; Sanchez, C. *Chem. Commun.* **2004**, *20*, 2312.

Table 3. Stoichiometries of the Obtained Open-Cell Monoliths Organo-Si(HIPE) after $Eu(NO_3)_3 \cdot 5H_2O$ Impregnation

	weight percentage (%)				
sample	carbon[a]	nitrogen[a]	europium[a]	water weight loss[b]	stoichiometry
Eu^{3+}@β-diketone-Si(HIPE)	17.65 (17.94)	1.92 (2.01)	7.48 (7.28)	5.00 (5.00)	$Eu_{0.05}(NO_3)_{0.15} \cdot SiO_{1.87}(C_{12}O_2H_{11})_{0.13} \cdot 0.29H_2O$
Eu^{3+}@$g\beta$-diketone-Si(HIPE)	7.22 (7.41)	1.08 (1.08)	3.93 (3.91)	5.40 (5.33)	$Eu_{0.02}(NO_3)_{0.06} \cdot SiO_{1.96}(C_{12}O_2H_{11})_{0.04} \cdot 0.23H_2O$
Eu^{3+}@*g*malonamide-Si(HIPE)	5.94 (6.31)	3.00 (3.15)	5.88 (5.71)	5.10 (4.96)	$Eu_{0.03}(NO_3)_{0.04} \cdot SiO_{1.93}(C_6N_2O_2H_{11})_{0.07} \cdot 0.22H_2O$

[a] The number in parentheses corresponds to the weight percentage calculated while the number not in parentheses corresponds to the values extracted from elemental analysis. [b] The number in parentheses corresponds to the weight loss calculated while the number not in parentheses corresponds to the values extracted from TGA experiments.

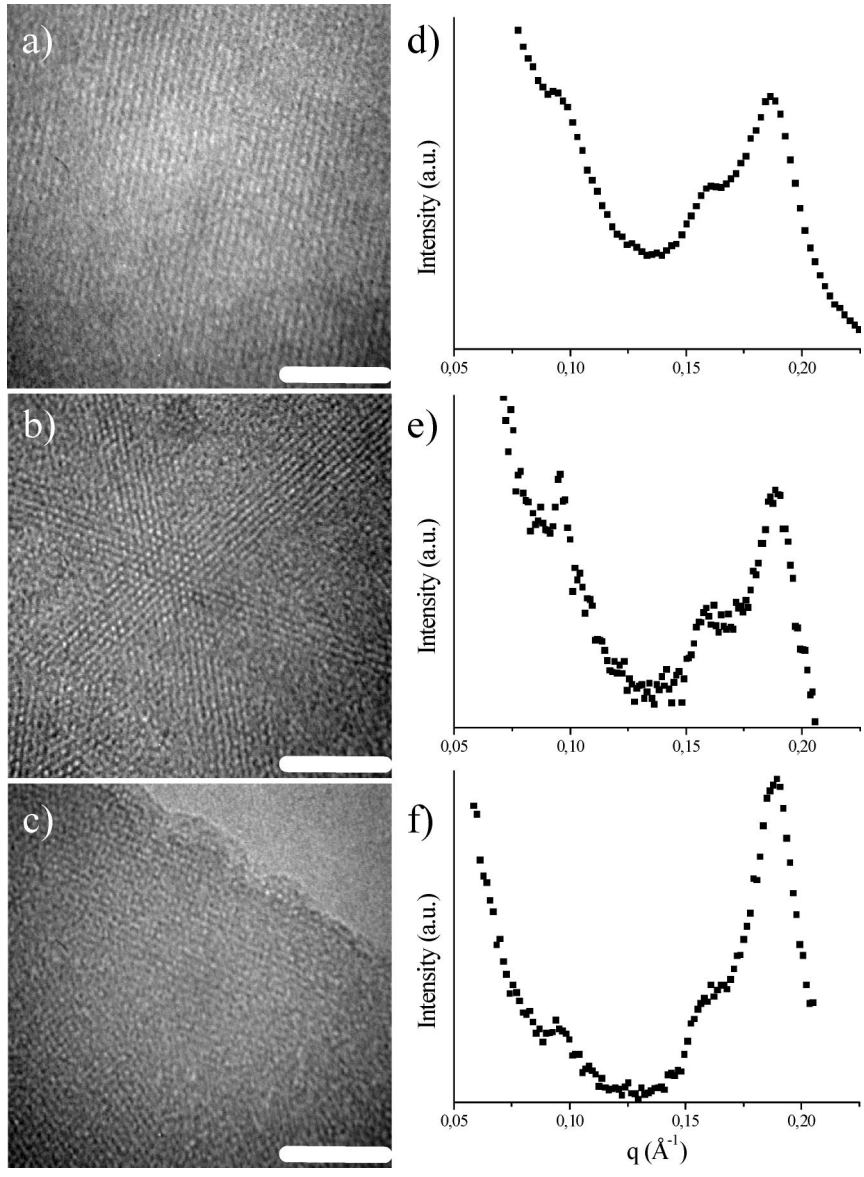

Figure 3. TEM micrographs: (a) Eu^{3+}@β-diketone-Si(HIPE), (b) Eu^{3+}@$g\beta$-diketone-Si(HIPE), and (c) Eu^{3+}@*g*malonamide-Si(HIPE). The scale bars represent 50 nm. SAXS diffusion profiles: (d) β-diketone-Si(HIPE), (e) β-diketone-Si(HIPE), and (f) *g*malonamide-Si(HIPE).

appear to be trimodal with two microporosities centered around 1.1 and 1.7 nm with an additional mesopororous contribution centered at 2.2 nm.

If we compare the nitrogen physisorption results that strongly suggest a mesopore diameter of 2.3 nm with the SAXS experiments that reveal a structural unit cell a_0 equals to 7.6 nm, there is, at first glance, a certain discrepancy as this should induce a wall thickness around 5 nm, and according to the TEM results and previous works the wall thickness is closer to 2 nm.[23] In fact we have to consider that the grafted entities cannot be seen through TEM observations while effectively minimizing the mesopore diameters reached through nitrogen physisorption measurements. In fact considering the length of both β-diketone and malonamide precusror derivatives (Scheme 1), around 1.4 nm we indeed recover a good interplay between TEM, SAXS, and N_2 physisorption results. If we add 2.3 nm of mesopores' diameter revealed by nitrogen sorption measurements, with two times the length of the silanes derivatives

(46) Chen, C. Y.; Xiao, S. O.; Davis, M. E. *Microporous Mater.* **1995**, *5*, 20.

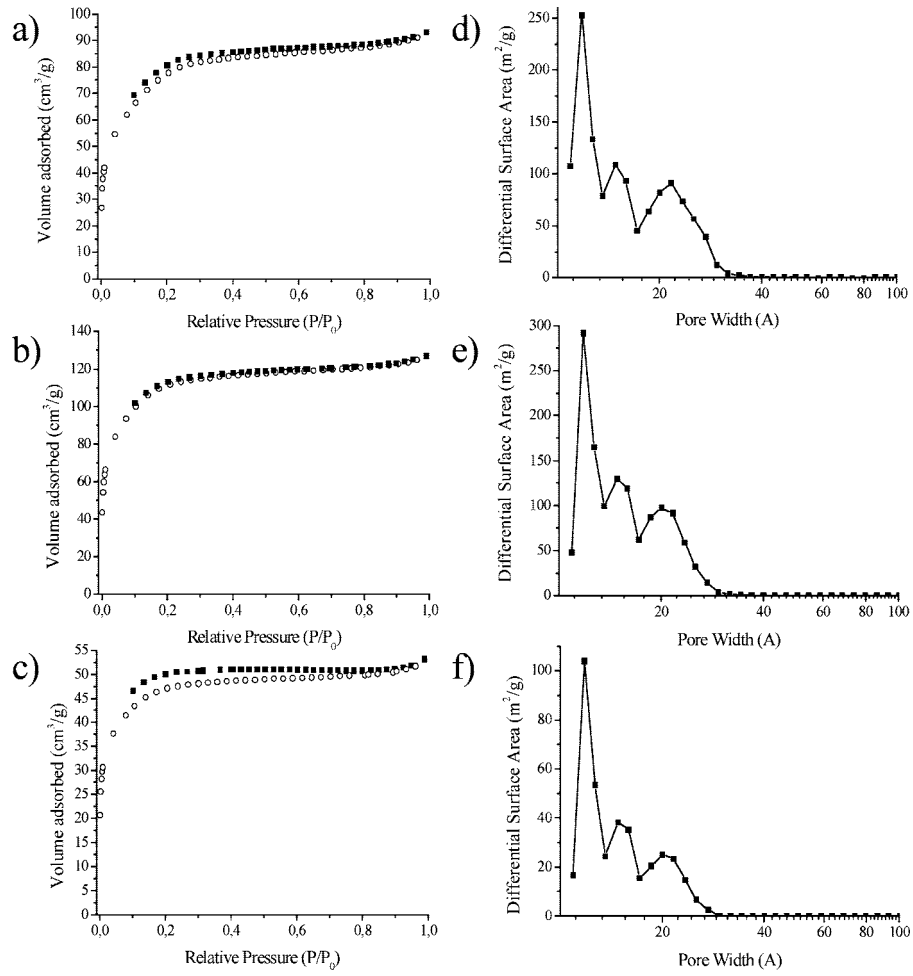

Figure 4. Nitrogen adsorption−desorption curves: (a) $Eu^{3+}@\beta$-diketone-Si(HIPE), (b) $Eu^{3+}@g\beta$-diketone-Si(HIPE), (c) $Eu^{3+}@g$malonamide-Si(HIPE). ○, adsorption curve; ■, desorption curve. Mesoscopic and microscopic pore sizes distribution obtained through the differential functional theory (DFT): (d) $Eu^{3+}@\beta$-diketone-Si(HIPE), (e) $Eu^{3+}@g\beta$-diketone-Si(HIPE), and (f) $Eu^{3+}@g$malonamide-Si(HIPE).

Scheme 1. (1) **N1-(3-(Triethoxysilyl)propyl)malonamide and** (2) **1-[4-(2-Triethoxysilyl-vinyl)-phenyl]-butane-1,3-dione**

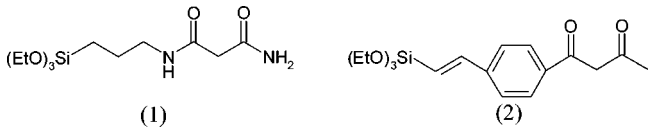

(2.8 nm, we hypothesized here homogeneous repartition of the organically modified silanes within the mesopores) and the silica wall thickness (around 2 nm), we almost recover the unit cell dimension (a_0) around 7.5 nm found under SAXS experiments.

To get information about the elemental composition of the materials we combined C, H, N, and Eu elemental analyses with thermogravimetry experiments (TGA) to address the content of structural water. The results are summarized within the Table 3.

Basically we can observe that the co-condensation process allows a higher amount of silane derivatives to associate to the silica network, when compared with the grafting process. As a direct consequence, the quantity of europium ions anchored within the matrices obtained through the one step co-condensation route is higher when compared with the ones obtained via the grafting method. The water content, in agreement with the europium salt hydration, is following the same evolution when comparing the grafting and the co-condensation obtained materials. Beyond stoichiometry, it is important to check the integrity of the organic components within final compounds as well as the europium sequestration that should influence vibration modes of the chelating agents to which it is coordinated. Therefore, we have employed Fourier transform infrared (FTIR) spectroscopy, and the spectra are depicted within the Figure 5.

The first observation is that all spectra have in common a strong absorption centered at 1076 cm^{-1} that corresponds to the ν(Si−O) stretching modes. The second vibration mode, present in the whole spectra, is the one involving the stretching mode of the Si−C link occurring within the 900−700 cm^{-1} region, and it occurs for the β-diketone-Si(HIPE) and malonamide-Si(HIPE) at 954 cm^{-1}. Also, the silanol (Si−OH) vibration mode is present at around 3250 cm^{-1} generating a superimposed shoulder among the resonance structures (hydrogen bonds) of the adsorbed water OH stretching modes (broader band ranging from 3200 to 3600 cm^{-1}). After Europium impregnation all the spectra possess the nitrate $\nu(NO_3^-)$ stretching modes signature at 1385 cm^{-1} (red arrow Figure 5). More independently each of the silane organic moieties should promote specific absorption modes acting as a molecule signature. Considering the IRTF

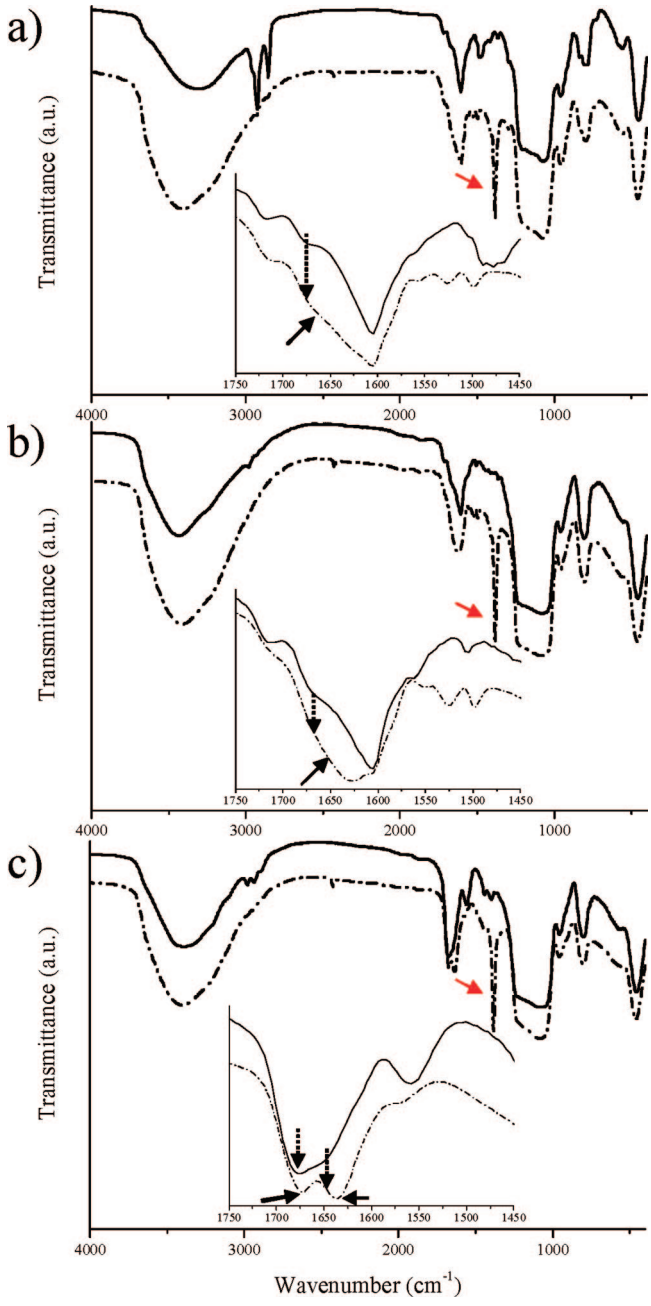

Figure 5. Organo-Si(HIPE) FTIR spectra: (a) β-diketone-Si(HIPE), (b) $g\beta$-diketone-Si(HIPE), and (c) *g*malonamide-Si(HIPE). Before europium impregnation (solid line), after europium impregnation (dashed line). The red arrows indicate nitrate stretching modes, the dashed black arrows indicate the remaining (C═O) vibration modes, and the solid arrows indicate new (C═O) vibration bands after Europium impregnation.

spectrum of the β-diketone-Si(HIPE) (Figure 5a, solid line) we can observe strong absorption at 2927 cm^{-1} and 2858 cm^{-1} that corresponds respectively to the symmetric $\nu_s(CH_2)$ and asymmetric $\nu_{as}(CH_2)$ stretching mode of the TTAB alkyl tails (in agreement with ^{13}C CP MAS NMR results, later in the text), that vanishes upon europium impregnation. This feature proves that the TTAB surfactant maintained within the organo-Si(HIPE) is washed out during the europium impregnation and final washing process. Therefore, a severe washing process, that is, three times with an isopropanol/ethanol mixture (at 50 vol %) during three days, allows a complete removal of the TTAB, which was not the case with previous compounds obtained through a one step co-

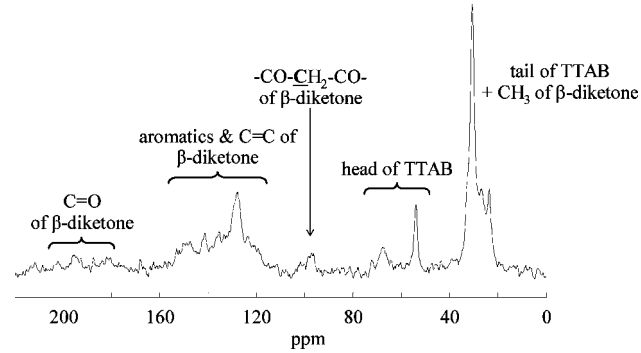

Figure 6. ^{13}C CP MAS NMR spectrum of the β-diketone-Si(HIPE) sample generated through the "one pot" synthesis, prior europium impregnation.

condensation process.[23] The FTIR spectra of the β-diketone-Si(HIPE) compounds (with or without europium), presented in Figure 6a,b, exhibits typical aromatic (C═C—C) weak stretching modes characterized by the presence of a group of four vibration bands located between 1450−1650 cm^{-1}. The europium complexation can be observed by analyzing the (C═O) stretching modes that vibrates in the 1600 cm^{-1}/1700 cm^{-1} frequency range. This characteristic feature is addressed for all compounds as embedded figures within the Figure 6. Concerning the β-diketone silane derivatives (Figure 5a,b), they offer both upon europium impregnation a partial shift of the ν(C═O) stretching mode from 1669 cm^{-1} to 1629 cm^{-1}, in good agreement with the literature.[47] In our case we observed both shifted and unshifted ν(C═O) vibration resulting in a peak broadening. This result, which reflects that some carbonyl function remains uncoordinated to europium ions, is in agreement with the compound stoichiometry reported in Table 3. We can observe that in Eu@β-diketone compounds are bearing two ligands per europium. Concerning the spectrum of the malonamide silane derivative, such as all the primary amides, it displays a second band closely located to the main carbonyl absorption and it lies on the low frequency side in the range 1650 cm^{-1}−1620 cm^{-1}. This new band is in fact characteristic of the NH_2 deformation band; thereby the silane malonamide derivatives are depicting two main distinguishable adsorption bands within the 1600 cm^{-1}/1700 cm^{-1} wavenumbers region (Figure 5c, embedded). Upon europium impregnation, the shift of the high wavenumber C═O stretching mode to the lower frequencies is less expressed (shift from 1676 cm^{-1} to 1671 cm^{-1}), but the shift of the NH_2 deformation band frequency is more pronounced (shift from 1653 cm^{-1} to 1635 cm^{-1}). This feature indicates that concerning the malonamide the amine group is certainly contributing to the europium complexation that cannot be the case for the β-diketone silane derivative. Overall the FTIR results are showing that (i) the organic moieties of these new open-cell materials remain intact through the employed synthetic route, (ii) the sequestering of europium guests is effective, and (iii) there is a strong difference in the europium complexation when switching from the β-diketone silane derivative to the malonamide one.

(47) Franville, A.-C.; Zambon, D.; Mahiou, R. *Chem. Mater.* **2000**, *12*, 428.

Table 4. Attributions of the ^{13}C CP MAS NMR Spectrum to the β-Diketone and TTAB Species

	δ (ppm)						
	205−180	168	155−110	98	68	54	35−20
β-diketone	C=O	HC=*C*OH (enol)	aromatics + Si−C=C	HC=COH (enol)		OC−CH_2−CO	CH_3−CO
TTAB					N−CH_2	CH_3−N	CH_2−CH_2−CH_n

To have a better quantification of the TTAB content in the β-diketone-Si(HIPE) sample generated through the "one pot" synthesis and prior europium impregnation, we have recorded a ^{13}C CP MAS NMR spectrum (Figure 6).

Even if the CP technique is not quantitative, it shows that the amount of TTAB in this sample is quite significant as revealed on one side by the strong peaks between 20 and 35 ppm characteristic of the TTAB tail and on the other side by the peaks at 54 and 68 ppm characteristic of the polar head of the surfactant. When looking to the β-diketone part of the sample, no evidence of ethoxy group could be seen around 18 and 58 ppm, attesting for a complete hydrolysis. However, the peak at 98 ppm revealed that the β-diketone is at least partially in the enolic form. Also, the β-diketone weak carbonyl (C=O) peak is present around 180−210 ppm. As the grafted samples were first calcined at 650 °C, no TTAB could remain inside the sample, as confirmed by FTIR results (Figure 5) and thus the ^{13}C (Figure 6). The chemical shift attributions are summed up in Table 4.

Furthermore, the materials have been characterized by using ^{29}Si CP MAS NMR spectroscopy (Figure 7).

As was previously said, CP technique is not quantitative. Nevertheless, as the experimental conditions are identical and the samples very similar, the CP MAS experiment can be sufficient to compare the samples (Table 5). First of all, the chemical shift of the T species of the β-diketone-Si(HIPE) and $g\beta$-diketone-Si(HIPE) samples is shifted more than 10 ppm upfield compared to the *g*Malonamide-Si(HIPE) sample, due to the carbon double bond.

Analyzing the β-diketone-Si(HIPE) and the $g\beta$-diketone-Si(HIPE) samples, it comes that the T_3/T_2 ratio is higher for the one-pot synthesis than for the postgrafted materials. The T_3/T_2 ratio is comparable for both the *g*Malonamide-Si(HIPE) and $g\beta$-diketone-Si(HIPE) samples. These results indicate that the condensation of T species seems to be limited in the case of postgrafted samples. This is likely due to the geometric constrains that forbid the T species to be grafted by three oxygen atoms. Thus, the T species are mostly grafted by two oxygen atoms, forming a layer at the surface of the Q species. On the contrary, in the one-pot samples, T and Q species might be either interpenetrated or clusterized.

The optical properties of the Eu-doped Si(HIPE) materials were analyzed by different optical techniques. UV−vis absorption spectra of the three samples are shown in Figure 8. The absorption spectrum of the Eu@*g*malonamide-Si(HIPE) sample is characteristic of a white sample, with no absorption in the visible wavelength range (around 350−750 nm). Only two very weak bands appear at 394 and 465 nm. They can be assigned to the spin forbidden $^5D_0 \rightarrow {}^5L_6$ and $^5D_0 \rightarrow {}^5D_2$ intra-4f transitions of the Eu^{3+} ions, respectively. These bands are not shown in the spectra of the yellow β-diketone and β-*g*diketone-Si(HIPE) samples because they are blurred by other absorptions near the UV region.

The careful deconvolution of the three spectra revealed the presence of a strong absorption of the Si−O host matrix centered at ~210 nm and two more bands assigned to the complexing groups. In the sample with malonamide group, these absorptions are located at 275 and 302 nm, and in the samples with β-diketone groups, they are found at 268 and 350 nm. In both cases, the first signal can be attributed to the $\pi-\pi^*$ transition of chelating agents and the second one to the metal−ligand charge transfer band

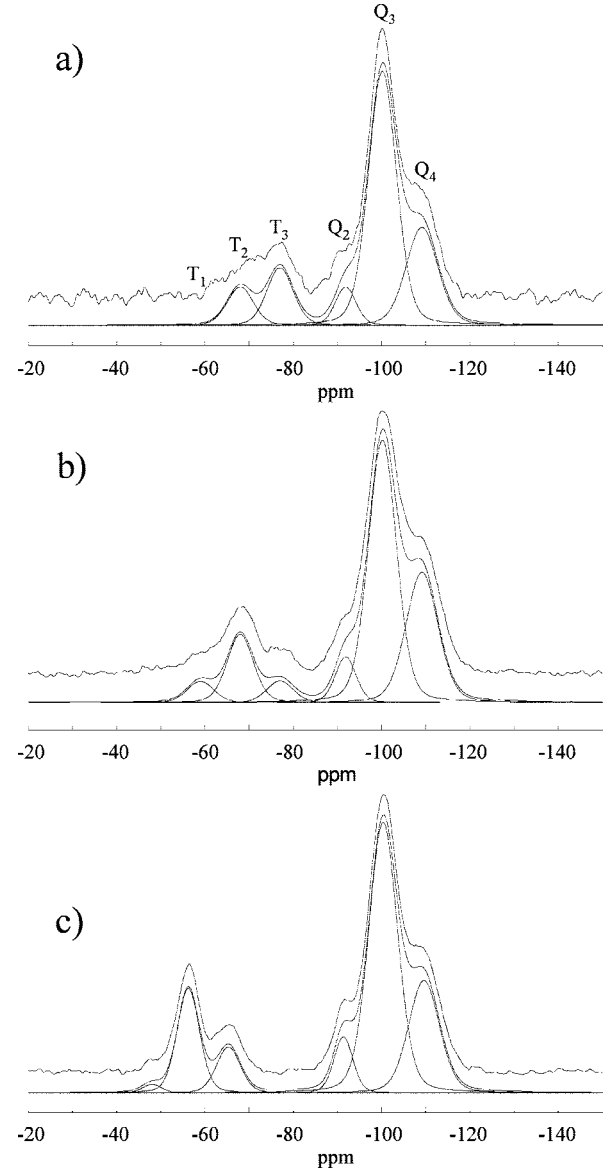

Figure 7. ^{29}Si CP MAS NMR spectroscopy spectra. (a) β-diketone-Si(HIPE), (b) $g\beta$-diketone-Si(HIPE), and (c) *g*Malonamide-Si(HIPE). Assignments of the signals to silane-derived species. The spectra were deconvoluted with the DMFIT program.[38]

Table 5. Summary of the ^{29}Si CP MAS NMR Samples Chemical Shift and Width

sample	T_1	T_2	T_3	Q_2	Q_3	Q_4	T_3/T_2	Q_4/Q_3
β-diketone-Si(HIPE)	−	7.4	11.2	5.8	52.6	22.9	1.5	0.44
chemical shift (ppm)	−59.0	−68.0	−77.0	−91.9	−100.2	−109.1		
width (ppm)	7.0	7.0	7.0	5.5	7.5	8.5		
$g\beta$-diketone-Si(HIPE)	3.6	11.6	3.7	6.1	48.0	27.0	0.32	0.56
chemical shift	*−59.0*	−68.0	−77.0	−91.9	−100.2	−109.1		
width (ppm)	*7.0*	7.0	7.0	5.5	7.5	8.5		
*g*Malonamide-Si(HIPE)	1.1	14.4	6.9	6.7	49.1	21.7	0.48	0.44
chemical shift	−48.8	−56.3	−65.3	−91.4	−100.3	−109.6		
width (ppm)	5.0	5.8	6.4	5.1	7.7	8.2		

(MLCT) after Eu coordination to the complexing groups. This red shift is a typical behavior of bidentate chelates when bonded to metal cations through the C=O groups.[48] This result is in complete agreement with the FTIR measurements in which both shifted and unshifted vibration bands of the carbonyl groups pointed to the presence of free chelating groups. Room-temperature excitation spectra of Eu-doped Si(HIPE) materials monitored around the more intense emission line of the Eu^{3+} at 615 nm are shown in Figure 9. With the aim of comparing the optical features, the spectra were normalized by one of the bands located out of the matrix or complex absorption, that is, at 465 nm.

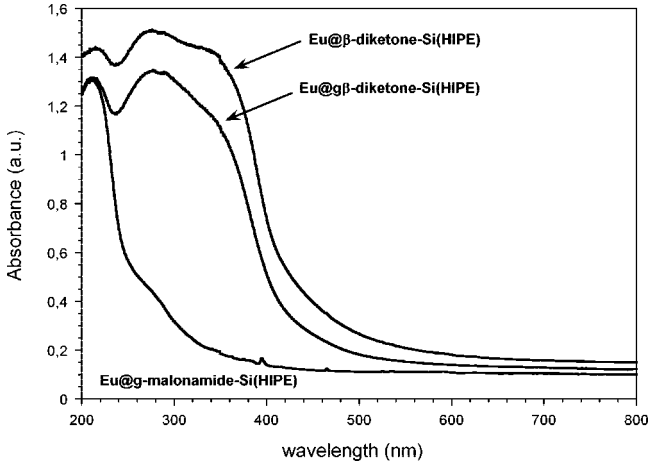

Figure 8. UV−vis absorption spectra of the Eu-doped organically derived Si(HIPE) hybrid materials.

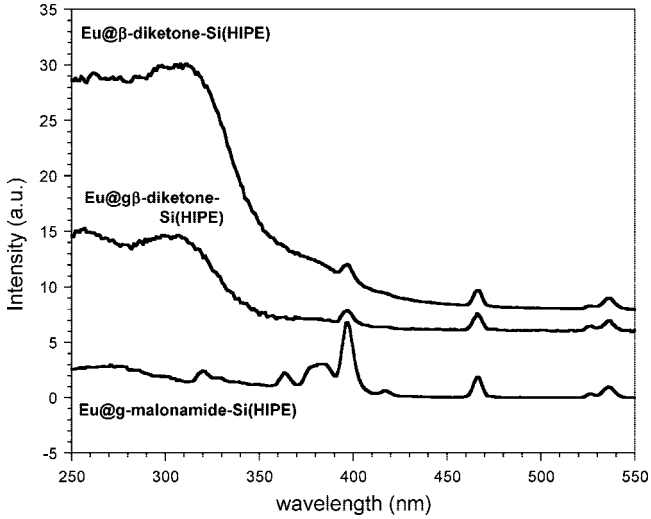

Figure 9. Excitation spectra of the Eu-doped organically derived Si(HIPE) hybrid materials monitored the Eu^{3+} emission at 615 nm.

All spectra exhibit the signals characteristic of the f−f transition levels (assigned in the figure) of the lanthanide ion. However, depending on the nature of the complexing group, important differences in intensity and in the profile are appreciated. Indeed, the spectra of both β-diketone derived compounds are dominated by the intense absorption in the UV and blue region, which can be assigned to the $\pi \rightarrow \pi^*$ excitation of the ligand, thus reducing the direct excitation of the Eu^{3+} energy levels. This behavior is especially important in the sample prepared by a co-condensation of the TEOS and organically derived precursors, indicating that the charge of chelating agent in the Si(HIPE) foam is higher, as already revealed by elemental analysis. In this situation, the energy is mainly absorbed by the lowest triplet level of the β-diketone ligand and efficiently transferred to the resonance energy level of the central Eu^{3+} ion. In contrast, for the Eu@*g*malonamide-Si(HIPE) sample, a weaker band is detected around 275 nm. It indicates that the excitation bands of Eu(III) in the UV region are less affected by the complexation with malonamide groups. It could be explained by the low energy overlapping between the absorption levels of Eu and this ligand, as observed in the absorption spectrum.

The photoluminescence emission spectra (PLE) of the Eu^{3+} organically derived Si(HIPE) materials were obtained using two different excitation wavelengths corresponding to the absorption maximum positions of the ligands (270 and ~305 nm for malonamide and β-diketonate, respectively) and the most intense excitation of the Eu^{3+} (396 nm). As an example, the spectra registered for the Eu@β-diketone-Si(HIPE) sample is shown on the left side of Figure 10. They consist of a set of emission lines corresponding to the intra 4f electronic transitions from the lowest excited state, $^5D_0$, to the ground-state manifold, ^7F_J ($J = 0-4$). Upon ligand excitation, from the analysis of the absorption bands in Figure 9, a great enhancement of the PLE emission is detected for the sample prepared in a one-pot process in comparison with the analogue synthesized by the grafting process. This result can be explained in terms of the more effective energy transfer between the complexing ligand and the Eu^{3+} ion. This effect is really interesting for the design of light emitting

(48) (a) Chan, G. Y. S.; Drew, M. G. B.; Hudson, M. J.; Iveson, P. B.; Liljenzin, J.-O.; Skalberg, M.; Spjuth, L.; Madic, C. *J. Chem. Soc., Dalton Trans.* **1997**, 649. (b) Edwards, H. G. M.; Hickmott, E.; Hughes, M. A. *Spectrochim. Acta, Part A* **1997**, *53*, 43. (c) Weihua, Z.; Gaoyang, Z.; Zhiming, C. *Mater. Sci. Eng.* **2003**, *B99*, 168.

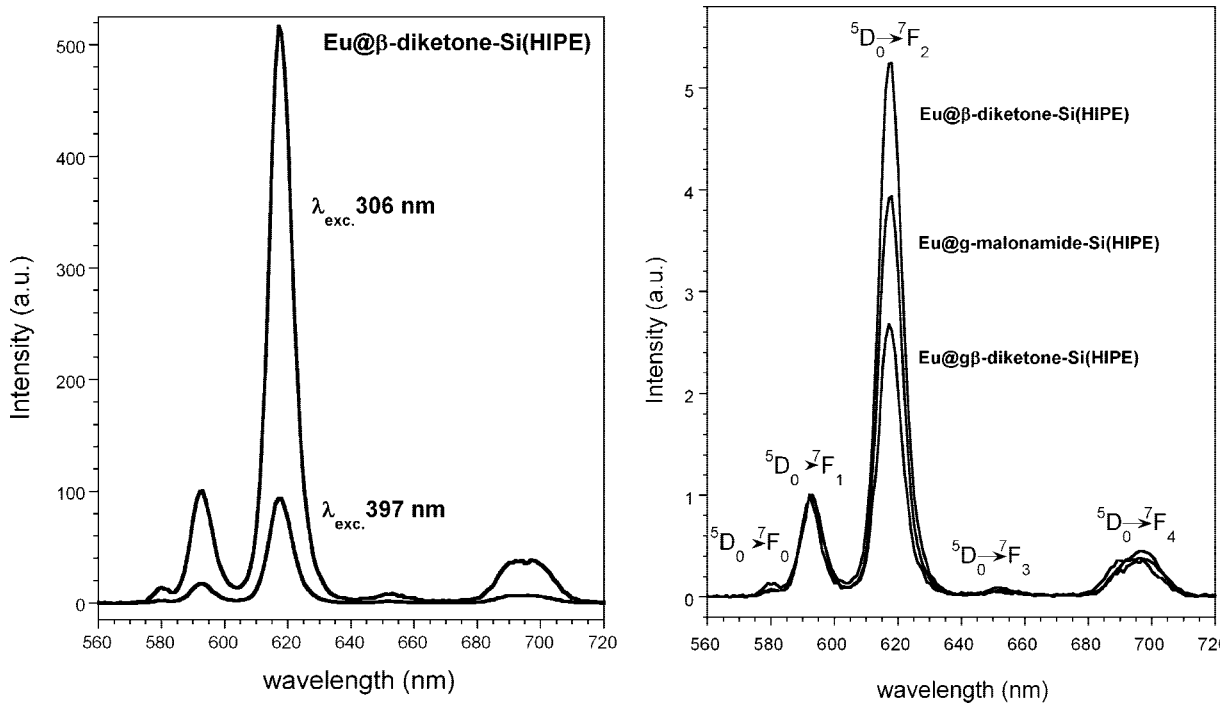

Figure 10. Emission spectra of (left) the Eu@β-diketone-Si(HIPE) upon Eu^{3+} excitation and (right) those of the three samples upon ligand excitation after normalization. The emission spectra for the three Eu-doped organically derived Si(HIPE) upon ligand and Eu^{3+} excitation are in the Supporting Information (Figure 1).

devices since the aim is to find a high efficiency in the PLE spectrum. For the Eu^{3+}@gmalonamide-Si(HIPE), a high emission intensity is also observed, but upon excitation at the Eu $^5L_6$ level, in accordance with the excitation spectrum (emission spectra not shown). Thus, depending on the excitation wavelength, the stronger PL intensity can be achieved through complexation by the β-diketone (excited at 306 nm) or the malonamide chelate (excited at 396 nm).

In addition, some of the Eu(III) emission bands being sensitive to changes in the first coordination sphere are particularly useful analytical tools. In particular, the intensity of the electric dipole $^5D_0 \rightarrow {}^7F_2$ transition ($\sim$615 nm) is known to be hypersensitive, and consequently, each spectrum has been normalized against the magnetic dipole $^5D_0 \rightarrow {}^7F_1$ transition, located at $\sim$590 nm, which is not affected by the environment of the fluorescent ion. The normalized spectra of the three samples after ligand excitation are depicted on the right in Figure 10.

The intensity of the electrical dipole transition increases when the lattice environment is distorted and contains certain components of noninversion symmetry. Thus, the ratio between the areas of the $^5D_0 \rightarrow {}^7F_2$ and $^5D_0 \rightarrow {}^7F_1$ transition bands can be considered as a parameter to probe the "asymmetry" of the Eu sites, and it is a good measure of the strength of the interaction between Eu(III) and the ligands. The spectra were fitted by Gaussian curves, and the ratio values obtained were 6.8, 4.7, and 3.5 for the Eu^{3+}@β-diketone, Eu^{3+}@$g\beta$-diketone, and Eu^{3+}@$g$malonamide-Si(HIPE)s, respectively. Note that these values were very similar to those obtained upon excitation at 396 nm, which indicates that Eu ions are mainly occupying a unique site in each system. Comparing the sensitive ratio for the two samples with β-diketone ligands indicates that Eu ions are located in a more asymmetric environment when prepared via a one-pot process than via the grafting one. In the case of the malonamide chelated sample, the symmetry of the Eu coordination is intermediate. The interpretation of these results are quite difficult since it is important to bear in mind that the Eu coordination (at least 8 fold coordination) cannot be satisfied uniquely with the bidentate chelating agents because the experimental chelate/Eu stoichiometry ratio is found to be between 2 and 3 that yield in the best case a maximum of six for Eu (III) coordinence number. Consequently, other species such as OH or nitrate groups are likely located in the first coordination sphere of the active lanthanide cation. The presence of these species in the final materials has been demonstrated by FTIR and elemental analysis but it is difficult to quantify their location is the lanthanide coordination sphere in order to extract straightforward conclusions concerning the symmetry of the Eu ions in the three materials.

Finally, decay curves were recorded upon chelate excitation in the UV region or upon direct excitation of Eu ions at 394 nm, with the fixed detection at the most intense emission wavelength of Eu^{3+} (615 nm). The luminescent relaxation profiles (figures not shown) were almost single exponential ($\ln I(t)\alpha - 1/\tau$, were $I(t)$ is the luminescence intensity in function of time and τ is the lifetime value), indicating that the Eu ions occupy the same average coordination environment. The lifetime values obtained by fitting are given in Table 6.

The lifetime values are io the order of hundreds of microseconds, between 110 and 460 μs, which are in agreement with the values registered for Eu(III) covalently

Table 6. Lifetime Values of the Eu^{3+}@Organo-Si(HIPE) Samples

	sample		
	Eu@β-diketone Si(HIPE)	Eu@$g\beta$-diketoneSi (HIPE)	Eu@g malonamideSi (HIPE)
τ (μs) (excited 394Eu)	110	130	450
τ (μs) (excited ligand)	150	150	460

bonded to chelates (100−600 μs).[49] It is interesting to point out that the Eu@gmalonamide-Si(HIPE) sample presents longer luminescent lifetimes than those of the samples containing the β-diketone ligand. This result could indicate that the binding of the Eu^{3+} ion to the malonamide through carbonyl amide groups, instead of the carbonyl groups of the β-diketone, may restrict the vibration of the ligand and improve the corresponding luminescence stability. Another interesting observation is that the values are independent of the excitation wavelength, which could be again explained by this probable rigidity of the Eu(III)−chelate bonds.

In general, lifetime values are extremely sensitive to the constitution of the active ion coordination sphere. Particularly, the lifetime of the $^5D_0$ level of the Eu^{3+} site is very sensitive to the hydroxyl groups concentration.[50] The OH groups are well-known quenchers of the luminescence since they absorb near Eu^{3+} emission, favoring nonradiative relaxation phenomena, and thus lifetime is expected to be shortened. The Eu@Organo-Si(HIPE) samples have not been thermally treated, so the inner shell of the Eu ions must certainly contain these quenching species, as already observed by FTIR. Therefore, the lifetime and the efficiency of the energy transfer between the excited ligand and the Eu^{3+} ion must be limited by the presence of OH groups.

Another factor to take into account in the optical efficiency is the formation of Eu^{3+} clusters. The poor solubility of lanthanide cations (Ln^{3+}) in the silica matrix and in the inorganic/organic media can lead to the lanthanide aggregation to satisfy its coordination. This effect is responsible for the low amplification property and is ascribed to the cooperative energy-transfer processes (i.e., self-quenching process) between the clustered Ln^{3+} species, thus reducing the intensity of luminescence. For this reason, it is important to incorporate chelating luminescent ligands which act as a sensitizer that transfers excitation energy to the embedded Ln^{3+} ion. In our systems, the elementary analysis reveals that the amount of chelates are in excess with respect to the Eu ions. Therefore, we can consider that europium ions are mostly complexed by the chelates, where the dual presence of OH groups and diverse ligand nature could be responsible for the differences observed in the decay times. Further investigations would be necessary to reveal more precise information on this subject.

Moreover, this new series of luminescent Eu^{3+} complexed Organo-Si(HIPE) materials is bearing a wide range of promising applications in catalysis, optics, sensors, absorbers, and so forth. We actually intend to express, beyond luminescent properties, these materials heterogeneous catalysis performances under the Michael reaction, and those results are in progress and will be published in due course.

Conclusion

Organosilica-based hybrid monoliths exhibiting a hierarchically structured bimodal porous structure with chelating functionality have been synthesized under dual templating processes that make the use of high internal phase emulsion (HIPE) and lytropic mesophases. Through a grafting process first Eu^{3+}@$g\beta$-diketone-Si(HIPE) and Eu^{3+}@$g$malonamide-Si(HIPE) hybrid compounds have been synthesized while the Eu^{3+}@β-diketone-Si(HIPE) material has been also synthesized through a one-step co-condensation process. The resulting materials have been thoroughly characterized via a large set of techniques: SEM, TEM, SAXS, mercury porosimetry, nitrogen adsorption isotherms, FTIR, and ^{29}Si and ^{13}CMAS NMR. The first results on optical properties of these versatile materials bearing macro- and microporosity have been addressed through their adsorption and emission spectra along with their relaxation luminescence properties. However, the establishment of basic principles of luminescence amplification, including the dependence with the ligand structure and the Ln^{3+} concentration on the efficiency and lifetimes, as well as the elucidation of basic energy transfer mechanisms needs further investigations still to fully appreciate their structure−property relationships.

Acknowledgment. This research was supported in part by the Spanish government (MAT2005-00541) and Bancaixa Foundation-Universitat Jaume I (P1 1B2007-47). B. Julián-López specially thanks the financial support of the Spanish government for the "Ramon y Cajal" program.

Supporting Information Available: Emission spectra of the three Eu-doped organically derived Si(HIPE) upon ligand and Eu^{3+} excitation (PDF). This material is available free of charge via the Internet at http://pubs.acs.org.

CM8018023

(49) (a) Li, Y.; Yan, B.; Yang, H. *J. Phys. Chem. C* **2008**, *112*, 3959. (b) Franville, A. C.; Mahiou, R.; Zambon, D.; Cousseins, J. C. *Solid State Sci.* **2001**, *3*, 211. (c) Costa, V. C.; Vasconcelos, V. L.; Bray, K. L. *Química Nova* **1998**, *21*, 374.

(50) (a) Meltzer, R. S.; Yen, W. M.; Zheng, H.; Feofilov, S. P.; Dejneka, M. J.; Tissue, B.; Yua, H. B. *J. Lumin.* **2001**, *94*, 217. (b) Nogami, M.; Hayakawa, T. *Phys. Rev. B* **1997**, 56–R14235. (c) Devlin, K.; O'Kelly, B.; Tang, Z. R.; McDonagh, C.; McGilp, J. F. *J. Non-Cryst. Solids* **1991**, *135*, 8.